4 $^{40}Ar/^{39}Ar$ geochronology in the Yuka HP/UHP terrane, North Qaidam*

4.1 Introduction

Over the last 15 years, a considerable number of studies with regard to petrological, geochemical and geochronological evolution of the North Qaidam HP/UHP orogenic belt has been carried out (Yang et al., 1994; Yang et al., 2001; Chen et al., 2005; Song et al., 2005a; Zhang et al., 2005a; Mattinson et al., 2006; Zhang et al., 2007; Mattinson et al., 2009; Menold et al., 2009; Zhang et al., 2009a; Zhang et al., 2010; Liu et al., 2012; Xiong et al., 2012). Based on the data of these previous studies, a number of mechanisms of subduction and exhumation, as well as models for the tectonic evolution of the orogen have been proposed (Yang et al., 2002a; Gehrels et al., 2003; Song et al., 2006; Xu et al., 2006; Yin et al., 2007; Song et al., 2014). However, the petrological and tectonic evolution North Qaidam orogen is still not fully understood. In particular, the ages of HP amphibolite-facies retrogression and cooling remain controversial, to an extent, due to the presence of extraneous ^{40}Ar. As a consequence there is a lack of appropriate age constraints on the mechanism of exhumation. Hence, further detailed thermal-geochronological analyses on representative minerals from both eclogites and their country rocks are desirable in order to derive new critical constraints on the pressure-temperature-time (*P-T-t*) path for these HP/UHP rocks.

The $^{40}Ar/^{39}Ar$ isotope dating technique is widely applied to date metamorphic events and related deformation to assess the cooling and exhumation history of orogenic belts. Since different minerals have different closure temperatures, it has become possible to date the final cooling through a specific closure temperature of a range of common minerals, which potentially allows the reconstruction of the cooling history of a rock unit (Dodson, 1973; Villa, 1998; McDougall and Harrison, 1999; Di Vincenzo and Palmeri, 2001; Hacker et al., 2011).

In this chapter, we present $^{40}Ar/^{39}Ar$ analyses of amphibole from eclogites and garnet amphibolites; phengite from eclogites, granitic gneiss and micaschist; and K-feldspar from granitic gneiss of the Yuka terrane, North Qaidam orogen. Combined with published U-Pb data, we attempt to (1) decipher the genesis of extraneous ^{40}Ar hosted in UHP metamorphic minerals; (2) constrain the cooling and exhumation history for the UHP rocks to upper-crustal depths by using new $^{40}Ar/^{39}Ar$ analyses and the commonly accepted values for the closure temperatures in different minerals.

* This chapter was part of the Chinese version of the thesis.

4.2 Previous geochronological work in the Yuka terrane

The Yuka eclogite-gneiss terrane is located in the westernmost segment of the North Qaidam UHP Orogen (Figure 4.1a). In the Yuka HP/UHP terrane, previous geochronological studies focused mainly on the UHP metamorphic rocks by applying zircon U-Pb dating with a variety of analytical methods and a primary focus on constraining the timing of peak UHP metamorphism (Zhang et al., 2005a; Chen et al., 2007a; Chen et al., 2009a; Song et al., 2010; Xiong et al., 2012).

U-Pb zircon ages of 495 ± 7 Ma and 488 ± 6 Ma (1σ error, TIMS) from two eclogites have been interpreted as representing the timing of eclogite-facies zircon growth based on inclusions of omphacite, garnet, and rutile (Zhang et al., 2000; 2005a). In contrast, Chen et al. (2009a) and Xiong et al. (2012) reported eclogite zircon (rim) U-Pb ages of 431 ± 4 to 443 ± 4 Ma (1σ error, LA-ICP-MS), which were regarded as documenting the timing of eclogite facies metamorphism. The conclusion was based on inclusions of rutile, garnet and omphacite in zircon, very low Th/U and Yb_N/Gd_N ratios, weak negative Eu anomalies, and flat heavy rare earth element patterns (HREE) of analyzed zircons. The inherited zircon core yielded U-Pb ages of ~750 – 800 Ma, which were interpreted as the protolith age of the eclogite supported by high Th/U and steep HREE patterns. Moreover, in situ SHRIMP II and SIMS U-Th-Pb analyses of zircon from two eclogite samples gave metamorphic ages of 433 ± 20 Ma with a relic core age of ~850 Ma (Song et al., 2010).

Constraints on the timing of retrograde metamorphism and exhumation are provided by ^{40}Ar/^{39}Ar cooling ages on amphibole and muscovite. Multigrain ^{40}Ar/^{39}Ar step heating measurements on amphibole and phengite from the eclogites yielded isochron ages of 477 ± 8 and 466 ± 5 Ma for cooling ages (2σ error), with initial ^{40}Ar/^{36}Ar ratios of 278.0 ± 37 and 352.9 ± 109, respectively (Zhang et al., 2000; 2005a).

Moreover, Menold (2006) investigated white mica fractions from eclogites as well as their country rock orthogneisses. Phengite separates from eclogites yield anomalously old apparent ages between 608 and 734 Ma, more than >100 Myr older than the previously established age of UHP metamorphism, indicating the presence of extraneous ^{40}Ar. On the other hand, white mica from orthogneisses gave apparent ages ranging from 419 to 824 Ma. Interestingly, white mica samples from within <1 m and > 5 m from the contact with the eclogite yield average apparent ages of 454 ± 4 Ma and 461 ± 6 Ma, respectively, whereas gneiss muscovite + paragonite from 1 – 5 m from the contact yield unreasonable apparent ages ranging from 610 – 824 Ma.

4.3 Sample description and mineral chemistry

Samples for Ar isotope analysis were collected along the northern bank of the Yuka River, Yuka terrane (Figure 4.1b), including phengite eclogites (09NQ08, 15, 18, 20 and 23), garnet amphibolites (09NQ13 and 29), micaschist (09NQ12) and granitic gneiss (09NQ24).

Samples 09NQ08, 15, 18, 20 and 23 are coarse-grained eclogites with granoblastic texture, comprising mainly garnet and omphacite with abundant sodic-calcic and calcic-amphibole and variable amounts of phengite, rutile, clinozoisite and quartz.

Amphibole is found in multiple textural environments: (1) early entrapped amphibole grains as inclusions (Amp-I) in garnet cores; (2) corona amphibole (Amp-II) around garnet rims; and (3) as a breakdown product of omphacite in the matrix (Amp-III). Amphiboles in the matrix that are separated for $^{40}Ar/^{39}Ar$ dating are classified as winchite and magnesio-katophorite with K/Ca mean ratios of 0.05 – 0.11 (see Table. 4.1).

Phengite occurs mainly associated with omphacite and clinozoisite in the matrix as an apparently texturally stable phase coexisting with the other eclogite facies minerals (Ph-II), or occasionally as inclusions in garnet mantles (Ph-I). Phengites in the matrix that were separated for $^{40}Ar/^{39}Ar$ dating all have compositions with Si of 3.34-3.57 per formula unit (p.f.u.), Mg/(Mg + Fe) ratios of 0.74-0.87 and Na/(Na + K) ratios of 0.03-0.13 (see Table. 4.2).

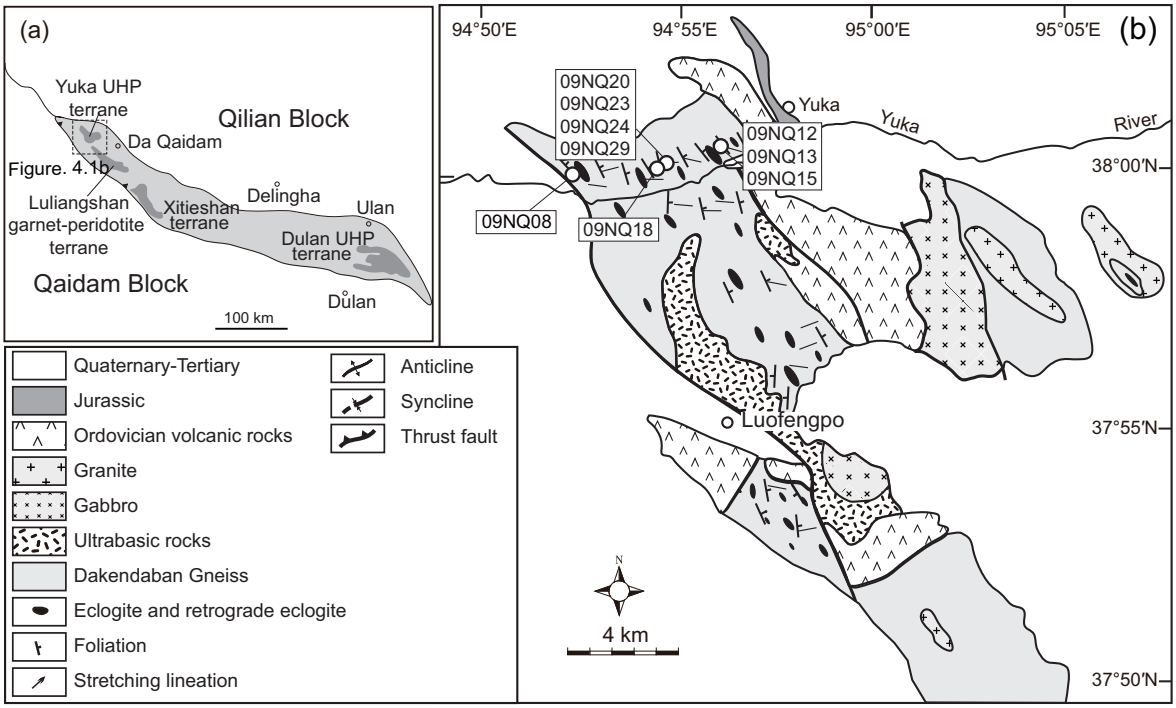

Figure 4.1 Regional map of the Yuka terrane and studied samples localities. Modified from Zhang et al. (2005a).

Samples 09NQ13 and 29 are medium- to coarse-grained garnet amphibolites, comprising amphibole, symplectite (Amp+Pl), epidote, plagioclase, quartz and garnet with minor titanite and zircon. Amphiboles are classified as tschermakite, edenite, winchite, magnesio-hornblende or barroisite with K/Ca mean ratios of 0.03 – 0.13 (see Table. 4.1).

Sample 09NQ12 is a strongly foliated schist made up of quartz and muscovite and with minor garnet porphyroblasts, clinozoisite and biotite. The foliation is defined by alignment of muscovite crystals up to 3 mm in size. Muscovite is characterized by a narrow range of compositions and a significantly lower Si content of 3.10-3.26 (p.f.u.). Their Mg/(Mg + Fe)

and Na/(Na + K) ratios range from 0.36-0.49 and 0.06-0.13, respectively (see Table. 4.2).

Table. 4.1 Microprobe analyses of Amphiboles from UHP metamorphic rocks in the Yuka terrane, north Qaidam*

Sample	09NQ08	09NQ13		09NQ15		09NQ29			
Spot	9	8	11	2	2	2	3	5	2
Mineral	Mg-ktp	Ed	Mg-hbl	Wnc	Mg-ktp	Wnc	Brs	Mg-hbl	Ts
SiO_2	46.68	43.94	45.51	53.45	47.00	53.76	52.64	47.67	42.45
TiO_2	0.50	0.46	0.40	0.11	0.53	0.10	0.10	0.20	0.34
Al_2O_3	14.59	13.84	11.98	3.87	11.71	7.88	8.82	10.60	17.55
FeO	10.92	14.85	14.31	11.03	12.92	4.57	4.99	11.60	11.77
MnO	0.03	0.13	0.19	0.03	0.03	0.04	0.05	0.25	0.26
MgO	11.66	9.76	10.59	16.01	11.52	17.99	17.51	12.98	10.97
CaO	8.80	10.37	10.68	9.54	8.69	8.81	8.90	11.31	10.47
Na_2O	3.83	2.35	1.75	1.99	3.70	2.60	2.65	1.53	2.49
K_2O	0.60	1.09	0.93	0.44	0.78	0.26	0.25	0.25	0.29
total	97.60	96.79	96.34	96.47	96.87	96.02	95.91	96.39	96.59
Si	6.71	6.55	6.78	7.71	6.89	7.52	7.40	6.96	6.23
Al^{IV}	1.23	1.39	1.18	0.28	1.05	0.47	0.59	1.01	1.73
Al^{VI}	1.24	1.04	0.92	0.38	0.97	0.83	0.87	0.81	1.30
Ti	0.05	0.05	0.04	0.01	0.06	0.01	0.01	0.02	0.04
$Fe^{(total)}$	1.31	1.85	1.78	1.33	1.58	0.54	0.59	1.42	1.45
Mn	0.00	0.02	0.02	0.00	0.00	0.00	0.01	0.03	0.03
Mg	2.50	2.17	2.35	3.44	2.52	3.75	3.67	2.82	2.40
Ca	1.36	1.66	1.70	1.47	1.37	1.32	1.34	1.77	1.65
Na	1.07	0.68	0.50	0.56	1.05	0.71	0.72	0.43	0.71
K	0.11	0.21	0.18	0.08	0.15	0.05	0.04	0.05	0.05
Cations	15.59	15.62	15.47	15.27	15.64	15.20	15.24	15.34	15.59
K/Ca	0.08	0.13	0.10	0.05	0.11	0.04	0.03	0.03	0.03

*Amphibole nomenclature after Leake et al. (1997). Mineral abbreviations are after Whitney and Evans (2010). Ed=edenite, Mg-hbl=magnesio hornblende, Wnc=winchite, Brs=Barroisite, Ts=tschermakite, Mg-ktp=magnesio katophorite.

Sample 09NQ24 is a medium-grained, banded and foliated granitic gneiss dominated by quartz, phengite, plagioclase, microcline with minor biotite. The foliation is formed by alignment of muscovite, parallel with the compositional banding. Phengite shows Si contents, Mg/(Mg + Fe) and Na/(Na + K) ratios of 3.27-3.32 p.f.u., 0.38-0.43 and ~0.03 (see Table. 4.2), respectively. Feldspars in the granitic gneiss are microcline ($Ab_{0.4-0.6}Or_{93-96}$) and albite ($Ab_{98}An_2$).

Table. 4.2 Microprobe analyses of phengite from high/ultrahigh metamorphic rocks in the Yuka terrane, North Qaidam

Sample	Eclogite (09NQ08)											Eclogite (09NQ18)							Eclogite (09NQ20)			
Mineral	Phengite											Phengite							Phengite			
Location	57	58	59	60	61	72	73	92	95	96	97	256	257	258	272	273	274	275	217	218	219	220
SiO_2	50.20	51.50	50.11	50.92	49.80	51.19	48.69	50.60	49.75	51.60	50.17	49.06	49.84	49.64	50.04	50.28	50.57	49.85	52.04	52.04	51.49	51.20
TiO_2	0.52	0.37	0.57	0.41	0.54	0.45	0.61	0.35	0.46	0.46	0.55	0.45	0.32	0.33	0.40	0.33	0.33	0.41	0.56	0.65	0.54	0.58
Al_2O_3	26.62	25.21	26.54	25.65	26.90	24.91	28.20	25.07	25.34	24.80	26.46	27.70	27.50	27.57	27.12	26.78	26.22	26.72	23.49	23.76	23.00	23.88
FeO	1.96	1.90	1.84	1.81	2.06	1.93	1.93	1.90	2.40	2.02	1.93	1.01	0.99	1.07	0.97	1.04	1.01	1.02	2.10	2.24	2.25	2.28
MnO	0.03	0.00	0.01	0.01	0.00	0.02	0.00	0.00	0.00	0.01	0.00	0.02	0.00	0.00	0.00	0.01	0.00	0.00	0.01	0.00	0.00	0.01
MgO	3.82	4.09	3.75	3.96	4.08	4.27	3.15	4.17	5.07	4.30	3.93	3.15	3.39	3.33	3.52	3.70	3.75	3.58	4.17	4.14	4.09	3.88
CaO	0.01	0.00	0.01	0.00	0.00	0.00	0.00	0.01	0.07	0.00	0.00	0.00	0.01	0.01	0.01	0.00	0.01	0.00	0.00	0.00	0.00	0.00
Na_2O	0.45	0.31	0.39	0.35	0.60	0.26	0.67	0.26	0.39	0.27	0.40	0.95	0.78	0.85	0.82	0.58	0.72	0.66	0.32	0.26	0.25	0.32
K_2O	10.32	10.49	10.51	10.49	9.83	10.67	9.97	10.70	9.77	10.60	10.46	9.71	10.03	10.03	9.97	10.42	9.98	10.29	10.55	10.67	10.73	10.64
total	93.93	93.88	93.73	93.59	93.81	93.69	93.21	93.07	93.26	94.05	93.90	92.04	92.86	92.83	92.84	93.15	92.59	92.53	93.23	93.76	92.34	92.78
Si	3.40	3.48	3.40	3.45	3.37	3.47	3.32	3.46	3.39	3.49	3.40	3.36	3.39	3.38	3.40	3.41	3.44	3.41	3.55	3.53	3.55	3.51
Al^{IV}	0.60	0.52	0.60	0.55	0.63	0.53	0.68	0.54	0.61	0.51	0.60	0.64	0.61	0.62	0.60	0.59	0.56	0.59	0.45	0.47	0.45	0.49
Al^{VI}	1.52	1.49	1.52	1.50	1.51	1.46	1.58	1.48	1.43	1.46	1.51	1.60	1.59	1.59	1.57	1.56	1.55	1.56	1.43	1.43	1.42	1.45
Ti	0.03	0.02	0.03	0.02	0.03	0.02	0.03	0.02	0.02	0.02	0.03	0.02	0.02	0.02	0.02	0.02	0.02	0.02	0.03	0.03	0.03	0.03
$Fe^{(total)}$	0.11	0.11	0.10	0.10	0.12	0.11	0.11	0.11	0.14	0.11	0.11	0.06	0.06	0.06	0.06	0.06	0.06	0.06	0.12	0.13	0.13	0.13
Mn	0.00	0.00	0.00	0.00	0.00	0.00	0.00	0.00	0.00	0.00	0.00	0.00	0.00	0.00	0.00	0.00	0.00	0.00	0.00	0.00	0.00	0.00
Mg	0.39	0.41	0.38	0.40	0.41	0.43	0.32	0.43	0.52	0.43	0.40	0.32	0.34	0.34	0.36	0.37	0.38	0.36	0.42	0.42	0.42	0.40
Ca	0.00	0.00	0.00	0.00	0.00	0.00	0.00	0.00	0.00	0.00	0.00	0.00	0.00	0.00	0.00	0.00	0.00	0.00	0.00	0.00	0.00	0.00
Na	0.06	0.04	0.05	0.05	0.08	0.03	0.09	0.03	0.05	0.04	0.05	0.13	0.10	0.11	0.11	0.08	0.10	0.09	0.04	0.03	0.03	0.04
K	0.89	0.90	0.91	0.91	0.85	0.92	0.87	0.93	0.85	0.91	0.90	0.85	0.87	0.87	0.86	0.90	0.87	0.90	0.92	0.92	0.94	0.93
Mg/Mg+Fe	0.78	0.79	0.78	0.80	0.78	0.80	0.74	0.80	0.79	0.79	0.78	0.85	0.86	0.85	0.87	0.86	0.87	0.86	0.78	0.77	0.76	0.75
Na/Na+K	0.06	0.04	0.05	0.05	0.09	0.04	0.09	0.04	0.06	0.04	0.06	0.13	0.11	0.11	0.11	0.08	0.10	0.09	0.04	0.04	0.03	0.04

Continue Table. 4.2

Sample	Eclogite (09NQ20)			Eclogite (09NQ23)					Schist (09NQ12)							Gneiss (09NQ24)						
Mineral	Phengite			Phengite					Muscovite							Phengite						
Location	225	226	230	167	168	169	171	172	5	6	7	8	9	10	15	17	18	19	20	25	26	30
SiO_2	50.82	50.99	52.35	48.75	48.50	48.65	48.31	47.52	47.17	48.53	47.86	46.67	46.16	49.23	48.49	49.64	48.37	48.82	50.35	48.85	49.78	48.66
TiO_2	0.70	0.57	0.54	0.28	0.38	0.36	0.32	0.37	0.33	0.28	0.27	0.22	0.41	0.40	0.38	0.38	0.38	0.46	0.48	0.47	0.38	0.41
Al_2O_3	24.60	24.06	22.82	25.59	26.01	26.77	26.34	26.59	30.61	33.93	34.83	35.41	32.29	33.85	33.84	28.34	29.06	29.07	29.76	28.50	28.93	27.69
FeO	2.28	2.32	2.37	1.53	1.57	1.55	1.42	1.62	2.20	2.93	2.46	2.16	2.44	3.05	2.72	5.41	5.33	5.37	5.09	5.45	5.27	5.32
MnO	0.01	0.00	0.00	0.04	0.00	0.00	0.00	0.00	0.00	0.00	0.00	0.00	0.00	0.00	0.00	0.00	0.00	0.02	0.00	0.02	0.03	0.00
MgO	3.68	3.88	4.21	3.91	3.50	3.61	3.81	3.73	1.06	1.27	1.03	0.68	1.16	1.26	1.45	2.09	1.86	1.92	1.93	1.96	1.91	2.26
CaO	0.00	0.01	0.01	0.00	0.01	0.00	0.00	0.00	0.00	0.00	0.01	0.00	0.01	0.03	0.01	0.01	0.04	0.00	0.01	0.00	0.00	0.03
Na_2O	0.35	0.30	0.25	0.56	0.51	0.64	0.62	0.58	0.61	0.73	0.73	0.93	0.67	0.78	0.44	0.21	0.20	0.22	0.24	0.19	0.20	0.24
K_2O	10.75	10.71	10.55	10.35	10.39	10.20	10.28	10.22	9.72	10.12	10.12	9.09	9.79	9.93	10.59	10.77	10.11	10.83	10.07	10.36	10.73	10.27
total	93.19	92.84	93.10	90.99	90.86	91.78	91.10	90.62	91.70	97.79	97.31	95.16	92.92	98.52	97.92	96.83	95.35	96.71	97.93	95.80	97.22	94.87
Si	3.48	3.50	3.57	3.41	3.39	3.37	3.37	3.34	3.26	3.16	3.13	3.10	3.16	3.18	3.16	3.32	3.27	3.27	3.30	3.29	3.31	3.31
Al^{IV}	0.52	0.50	0.43	0.59	0.61	0.63	0.63	0.66	0.74	0.84	0.87	0.90	0.84	0.82	0.84	0.68	0.73	0.73	0.70	0.71	0.69	0.69
Al^{VI}	1.46	1.45	1.41	1.51	1.54	1.55	1.54	1.54	1.75	1.76	1.81	1.87	1.77	1.75	1.75	1.55	1.59	1.57	1.60	1.56	1.57	1.54
Ti	0.04	0.03	0.03	0.01	0.02	0.02	0.02	0.02	0.02	0.01	0.01	0.01	0.02	0.02	0.02	0.02	0.02	0.02	0.02	0.02	0.02	0.02
$Fe^{(total)}$	0.13	0.13	0.14	0.09	0.09	0.09	0.08	0.10	0.13	0.16	0.13	0.12	0.14	0.16	0.15	0.30	0.30	0.30	0.28	0.31	0.29	0.30
Mn	0.00	0.00	0.00	0.00	0.00	0.00	0.00	0.00	0.00	0.00	0.00	0.00	0.00	0.00	0.00	0.00	0.00	0.00	0.00	0.00	0.00	0.00
Mg	0.38	0.40	0.43	0.41	0.36	0.37	0.40	0.39	0.11	0.12	0.10	0.07	0.12	0.12	0.14	0.21	0.19	0.19	0.19	0.20	0.19	0.23
Ca	0.00	0.00	0.00	0.00	0.00	0.00	0.00	0.00	0.00	0.00	0.00	0.00	0.00	0.00	0.00	0.00	0.00	0.00	0.00	0.00	0.00	0.00
Na	0.05	0.04	0.03	0.08	0.07	0.09	0.08	0.08	0.08	0.09	0.09	0.12	0.09	0.10	0.06	0.03	0.03	0.03	0.03	0.02	0.03	0.03
K	0.94	0.94	0.92	0.92	0.93	0.90	0.92	0.92	0.86	0.84	0.84	0.77	0.85	0.82	0.88	0.92	0.87	0.93	0.84	0.89	0.91	0.89
Mg/Mg+Fe	0.74	0.75	0.76	0.82	0.80	0.81	0.83	0.80	0.46	0.44	0.43	0.36	0.46	0.42	0.49	0.41	0.38	0.39	0.40	0.39	0.39	0.43
Na/Na+K	0.05	0.04	0.03	0.08	0.07	0.09	0.08	0.08	0.09	0.10	0.10	0.13	0.09	0.11	0.06	0.03	0.03	0.03	0.03	0.03	0.03	0.03

4.4 Results of new ^{40}Ar/^{39}Ar stepwise heating

The ^{40}Ar/^{39}Ar laser stepwise heating experiments of white mica (09NQ12, 20 and 24) and amphiboles (09NQ13 and 29) were carried out on a MAP-215-50 mass spectrometer in the VU University Amsterdam, and the phengites (09NQ08, 18, and 23), amphiboles (09NQ08 and 15) and K-feldspar (09NQ24) were analysed on a GVI-5400 mass spectrometer in the Guangzhou Institute of Geochemistry, Chinese Academy of Sciences.

The ^{40}Ar/^{39}Ar data were calculated and plotted using the ArArCALC2.50 software package (Koppers, 2002). The summarized results are shown in Table. 4.3. Analytical methods are described in Appendix A. The ^{40}Ar/^{39}Ar analytical results are listed in Appendix B. Age spectra and inverse isochrons (^{36}Ar/^{40}Ar vs. ^{39}Ar/^{40}Ar) for each of the samples are plotted in Figure 4.2 to Figure 4.7. Both the plateau and inverse isochron age uncertainties are given at 2σ level.

Table. 4.3 Sample locations and summary of new ^{40}Ar/^{39}Ar data from Yuka terrane, North Qaidam

Sample	Mineral	TGA (Ma, 2σ)	WA (Ma, 2σ)	Step (Total)	$^{39}Ar_k$ (%)	IIA (Ma, 2σ)	^{40}Ar/^{36}Ar	MSWD (IIA)	Notes
09NQ08	Amp	1148.7 ± 8.6	1042.6 ± 105.2	1-12(12)	100	713.9 ± 58.1	3943 ± 590	>100	-
09NQ13	Amp	545.7 ± 2.4	530.6 ± 8.8	4-17(17)	92.7	472.6 ± 7.2	3314 ± 360	0.06	-
09NQ15	Amp	639.7 ± 5.5	612.1 ± 40.2	1-16(16)	100	526.3 ± 20.1	829 ± 104	>100	-
09NQ29	Amp	642.6 ± 1.5	631.4 ± 21.9	2-17(17)	99.6	472.2 ± 3.3	1468 ± 18	0.33	-
09NQ08	Ph	558.9 ± 4.9	559.2 ± 6.7	1-9(9)	100	556.2 ± 6.1	415 ± 94	39.4	WM1
09NQ12	Ms	418.9 ± 2.0	418.1 ± 2.0	1-16(16)	100	418.1 ± 1.9	297 ± 6	2.3	WM3
09NQ18	Ph	558.9 ± 4.8	558.4 ± 7.4	1-16(16)	100	559.9 ± 5.7	275 ± 26	>100	WM1
09NQ20	Ph	708.3 ± 3.0	713.0 ± 17.2	1-16(16)	100	555.6 ± 39.9	14601 ± 18862	>100	WM1
09NQ23	Ph	554.6 ± 4.8	553.4 ± 9.3	1-12(12)	100	557.8 ± 6.3	218 ± 35	>100	WM1
09NQ24	Ph	454.1 ± 2.0	455.1 ± 2.1	4-15(15)	90.8	455.1 ± 2.1	283 ± 53	3.19	WM2
09NQ24	Kfs	278.9 ± 2.6	282.9 ± 2.7	9-17(17)	58.3	283.2 ± 2.7	266 ± 46	0.56	-

*TGA: total gas age; WA: weighted age; IIA: inverse isochron age; MSWD: mean square weighted deviation. WM1=eclogite white mica; WM2=granitic gneiss white mica; WM3=schist white mica

4.4.1 ^{40}Ar/^{39}Ar results for amphibole

Amphibole separates from the eclogites (09NQ08Amp and 09NQ15Amp) yielded strongly discordant release spectra. Individual apparent ages range up to as high as ~3.8 Ga, and the total gas ages range from 640 to 1149 Ma (Figure 4.2a and c). The K/Ca ratios of the two analyzed amphibole samples are constant with average values of 0.078 ± 0.003 and 0.058 ± 0.002, respectively. The nearly flat K/Ca spectra obtained from these two samples indicate that they are chemically homogenous. Data points in the isotope correlation diagrams (^{36}Ar/^{40}Ar vs. ^{39}Ar/^{40}Ar) exhibit negatively correlated relationship as well as higher initial ^{40}Ar/^{36}Ar ratios, but the data is too scattered to reveal reasonable isochron ages (Figure 4.2b and d).

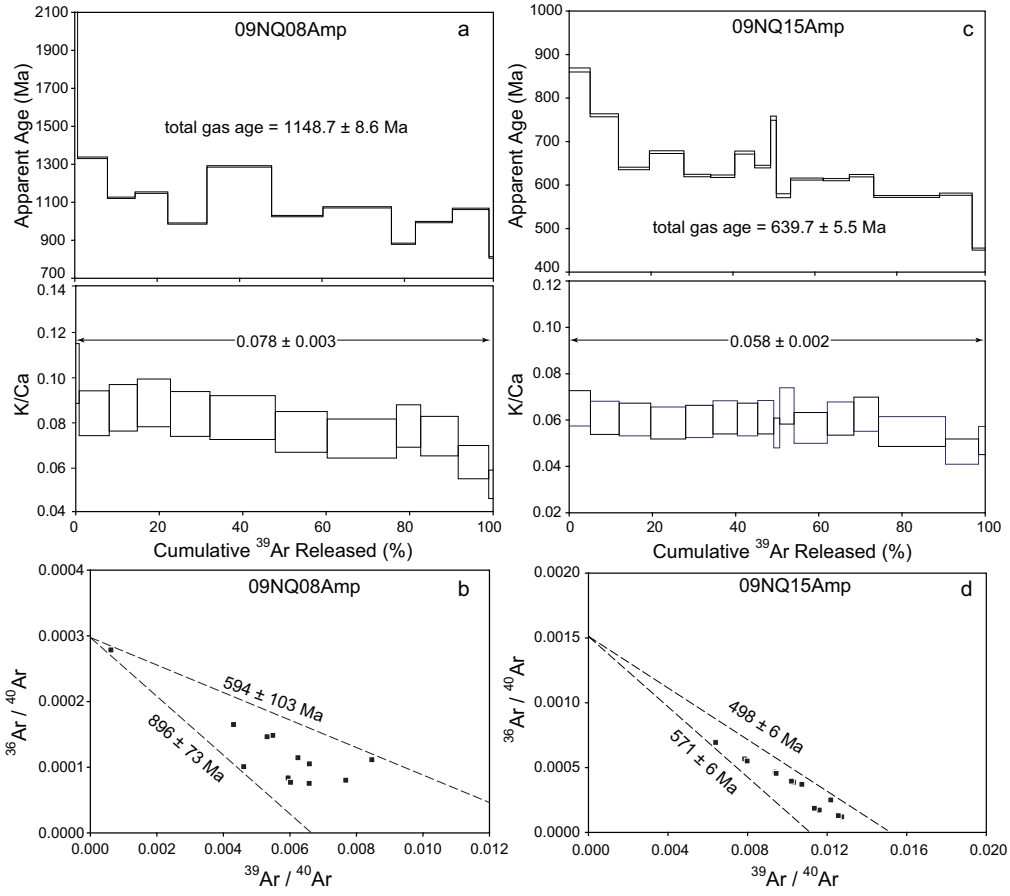

Figure 4.2 Apparent age spectra, K/Ca spectra, and inverse isochrons for amphiboles from eclogites from the Yuka terrane by laser stepwise heating. The error ellipses in the isochrons are too small to be shown. The dashed lines introduced here are not defined by the sequential data and only indicate the upper and lower boundaries of the data envelope. The data errors are in 2σ.

Amphibole separate 09NQ13Amp from the garnet amphibolite yielded a release spectrum with anomalously old apparent ages in the first few steps and a total gas age of 545.7 ± 2.4 Ma (Figure 4.3a). Nevertheless, the K/Ca spectrum is almost flat with a total gas value of 0.069 ± 0.004 (Figure 4.3a). In the $^{36}Ar/^{40}Ar$ vs. $^{39}Ar/^{40}Ar$ isotope correlation diagram, a subset of the data (4-17) reveals a good fit linear array with a younger isochron age of 472.6 ± 7.2 Ma, with a MSWD of 0.06 and an initial $^{40}Ar/^{36}Ar$ ratio as high as 3314 ± 360, reflecting the presence of extraneous ^{40}Ar (Figure 4.3b). Additionally, a significantly younger and flatter age spectrum is logically obtained once the apparent ages are recalculated using the $^{40}Ar/^{36}Ar$ ratio of the trapped components provided by the isochron (I_0 = 3314) for the corresponding heating steps, yielding a plateau age of 472.6 ± 4.3 Ma for approximately 92.7% of the total ^{39}Ar released (Figure 4.3a, dash line).

Amphibole 09NQ29Amp from the amphibolite exhibits a complex age spectrum but shows constant ratios in its K/Ca diagram once the initial four steps are excluded (Figure 4.3c). The release pattern is characterized by extremely high apparent ages in the initial steps and followed a crank-shaft shaped release pattern of the remaining segments, corresponding to a

total gas age of 642.6 ± 1.5 Ma (Figure 4.3c). Like in the previous sample, consecutive data points (2-17) define a linear array in inverse isochron diagram with an intercept age of 472.2 ± 3.3 Ma, with a corresponding MSWD of 0.33 and an initial ^{40}Ar/^{36}Ar ratio of 1468 ± 18 (Figure 4.3d). Again, a flatter spectrum and a concordant younger plateau age is logically obtained (472.2 ± 1.9 Ma) with approximately 99.6% of the total ^{39}Ar released once adopting the ^{40}Ar/^{36}Ar ratio (I_0 = 1468) from the isochron line to exclude the non-radiogenic ^{40}Ar (Figure 4.3c, dash line).

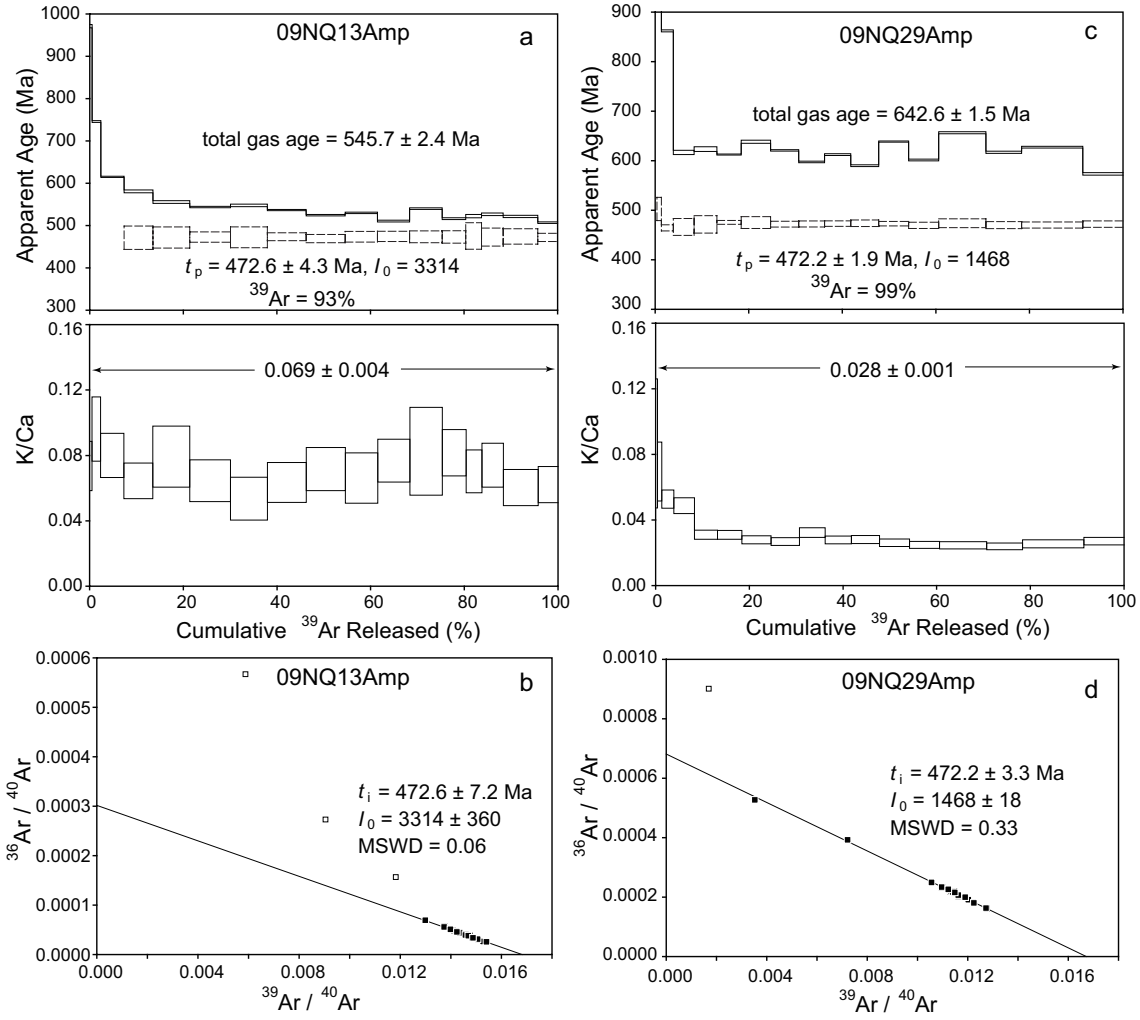

Figure 4.3 Apparent age spectra, K/Ca spectra, and inverse isochrons for amphibole from garnet amphibolites from the Yuka terrane obtained by laser stepwise heating. The older spectra (black line) were calculated assuming a trapped ^{40}Ar/^{36}Ar ratio of 295.5, while the spectra with younger ages (blue line) were calculated using the indicated ^{40}Ar/^{36}Ar ratio (I_0). On the inverse isochrons, the solid symbols are included in the calculations of plateau and isochron ages, while the open symbols are excluded. Errors are reported a 2σ.

4.4.2 ^{40}Ar/^{39}Ar results for phengite

Laser stepwise heating experiments were undertaken on six Yuka white mica samples.

Two samples from the country rocks yielded total gas ages of 418.9 ± 2.0 Ma and 453.4 ± 2.0 Ma, corresponding to precise plateau ages at 418.1 ± 2.0 Ma (09NQ12Ms) and 455.1 ± 2.1 Ma (09NQ24Ph) (Figure 4.4a and c), respectively. The data points constituting the age plateaux display well-defined isochrons and identical intercept ages of 418.1 ± 1.9 Ma ($^{40}Ar/^{36}Ar$ = 297 ± 6, MSWD = 2.4) and 455.1 ± 2.1 Ma ($^{40}Ar/^{36}Ar$ = 283 ± 53, MSWD = 3.2), respectively (Figure 4.4b and d).

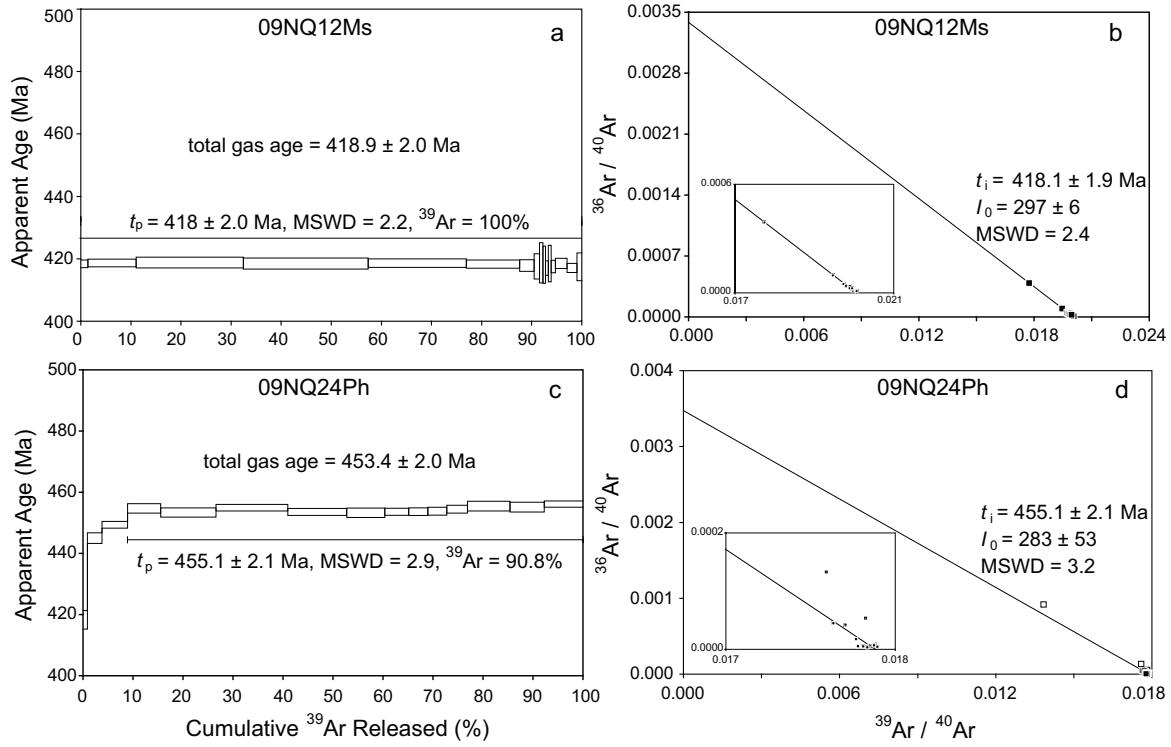

Figure 4.4 Apparent age spectra and inverse isochrons of white mica from the host schist and gneiss from Yuka terrane determined by laser stepwise heating. On the inverse isochrons, the solid symbols are included in the calculations of plateau and isochron ages, while the open symbols are excluded.

In contrast with the analyzed host rock phengites, phengites from the eclogites all show discordant apparent age spectra, with different shapes and unreasonable older total gas ages that range from 510 to 708 Ma (Figure 4.5a-d). The separates from the coarse-grained eclogites (09NQ08Ph, 09NQ18Ph and 09NQ23Ph) yield relatively flat age spectra and concordant total gas ages in the 555 – 559 Ma range, with individual apparent ages ranging 523 – 574 Ma (Figure 4.5a, b and d). Phengite from clinozoisite-rich eclogite 09NQ20 displays a complex age spectrum with anomalously old apparent ages (654 – 797 Ma) and a total gas age of 708 Ma (Figure 4.5c).

Because too many of the steps lie close to the $^{39}Ar/^{40}Ar$ axis and despite intensive efforts, the isotope correlation diagrams (see Figure 4.6a-d) do not allow to distinguish the extraneous ^{40}Ar and radiogenic argon, and reveal no systematic behavior for any of the spectra.

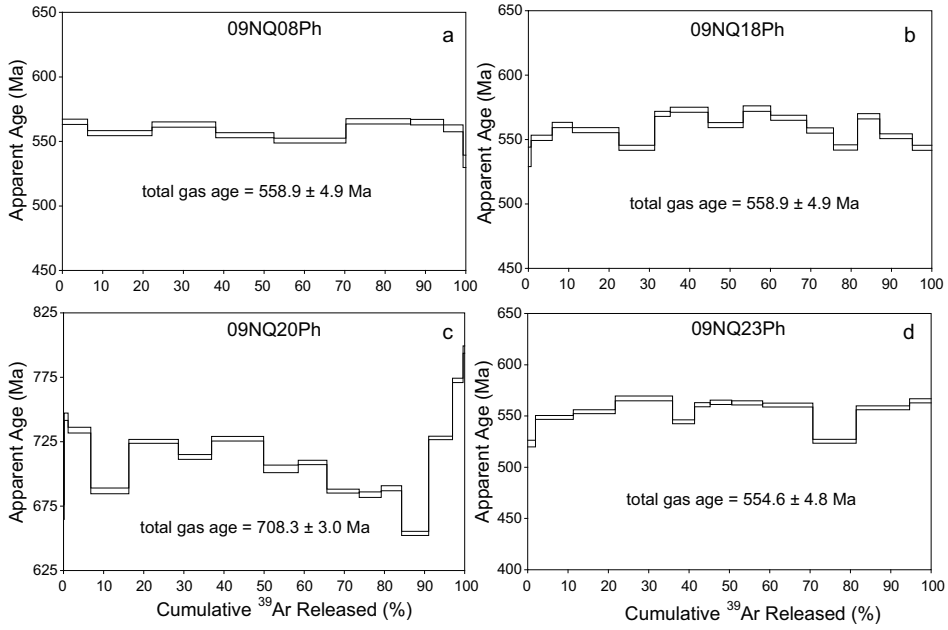

Figure 4.5 Apparent age spectra for phengite from Yuka eclogites with inhomogeneously distributed extraneous ^{40}Ar.

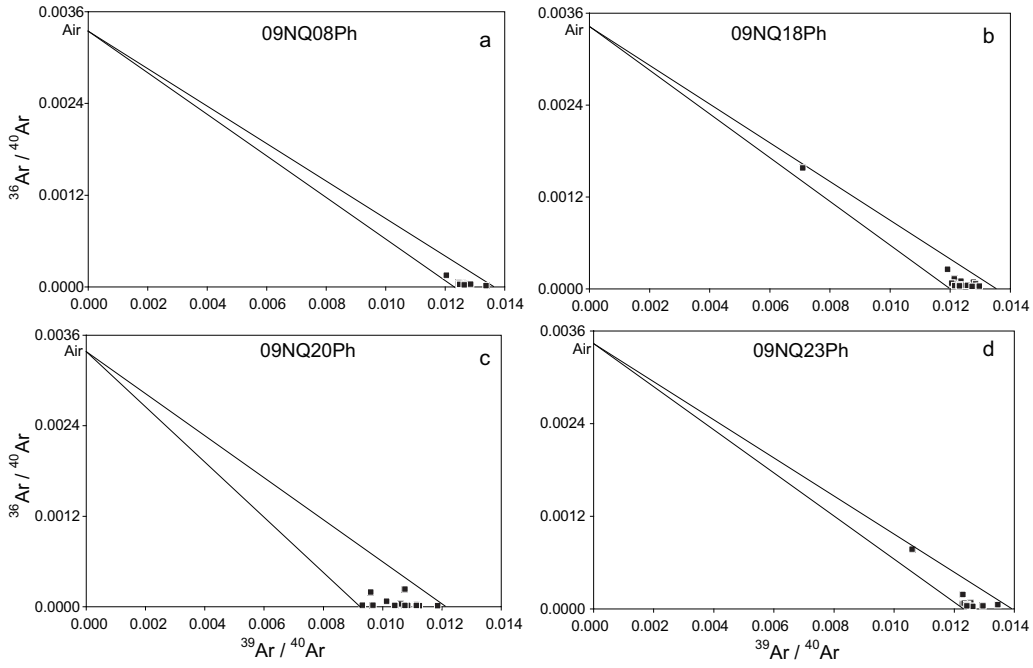

Figure 4.6 Inverse isochrons for phengite from Yuka eclogites with inhomogeneously distributed extraneous ^{40}Ar. The error ellipses in the isochrons are too small to be shown. The dashed lines introduced here are not defined by the sequential data and only indicate the upper and lower boundaries of the data envelope.

4.4.3 ^{40}Ar/^{39}Ar results for K-feldspar

The K-feldspar (09NQ24Kfs) was extracted from a granitic gneiss, and displayed a U-shaped spectrum with the oldest apparent age in the first step and the youngest apparent

age in the third step. The apparent ages increase from steps 3-8 which is followed by a flat section with plateau age of 282.9 ± 2.7 Ma, comprising 9 steps and 58.3% of the ^{39}Ar released (Figure 4.7a). Because of the highly radiogenic nature of ^{40}Ar from most steps (98.5-99.5%), the data cluster near the abscissa of the $^{36}Ar/^{40}Ar$ vs. $^{39}Ar/^{40}Ar$ isotope correlation diagram. Nevertheless, the data points constituting the age plateau still reveal a good fit isochron line with concordant intercept age of 283.2 ± 2.7 Ma ($^{40}Ar/^{36}Ar$ = 283 ± 53, MSWD = 0.56) (Figure 4.7b).

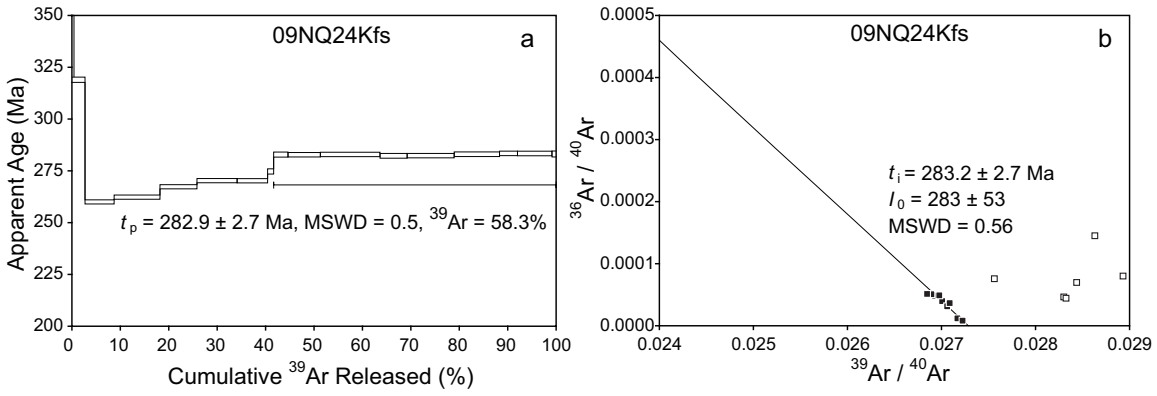

Figure 4.7 Apparent age spectrum and inverse isochron of K-feldspar from the Yuka gneiss by laser stepwise heating.

4.5 Discussion

There are several possible sources of argon of different isotopic composition present in geological samples. It is useful for the discussion to distinguish between excess, extraneous and inherited argon. Thus, before discussion, we present a nomenclature that was proposed by Dalrymple and Lanphere (1969) and restated by McDougall and Harrison (1999). According to the terminology proposed by Dalrymple and Lanphere (1969) and McDougall and Harrison (1999), extraneous argon, including excess and inherited argon, refers to the additional ^{40}Ar responsible for measured $^{40}Ar/^{36}Ar$ ratios >295.5, the value of this ratio in atmospheric argon. Inherited ^{40}Ar refers to any ^{40}Ar that is produced within mineral grains by the decay of ^{40}K before the event being dated. Excess ^{40}Ar is the component of ^{40}Ar that, together with atmospheric ^{40}Ar, is incorporated in rocks and minerals by processes other than *in-situ* radioactive day of ^{40}K.

4.5.1 Genesis of extraneous ^{40}Ar in Yuka phengite

The new laser stepwise heating analyses of high/ultrahigh pressure metamorphic phengite in Yuka eclogites underline the complicated nature of the behavior of argon isotopes during HP/UHP metamorphism and highly contrasting results were obtained for the different lithologies (Figure 4.8). For the new data we documented the link between lithology, chemical composition and argon isotope ages (Scaillet et al., 1992; Li et al., 1999).

Accordingly, phengite from the mafic eclogites (WM1, high-Si and Mg-rich, Figure 4.8) analyzed by laser stepwise heating yielded anomalously old discordant individual apparent ages (475 – 797 Ma) and total gas ages (554.6 – 708.3 Ma, Figure 4.5). These ages are significantly older than previously documented 488 – 495 Ma U-Pb zircon ages constraining peak metamorphism in the Yuka terrane (Zhang et al., 2005a), indicating the presence of extraneous ^{40}Ar. In contrast, stepwise heating of muscovite/phengite from the host rocks (WM2 and WM3, low-Si and Fe-rich, from schist and gneiss) yields flat release patterns and total gas ages of 418.5 Ma and 453.4 Ma (Figure 4.8).

The existence of extraneous ^{40}Ar in phengite from (U)HP metamorphic rocks is common (Li et al., 1994; Giorgis et al., 2000; Warren et al., 2012c; Smye et al., 2013). However, the genesis of extraneous ^{40}Ar is still a controversial issue.

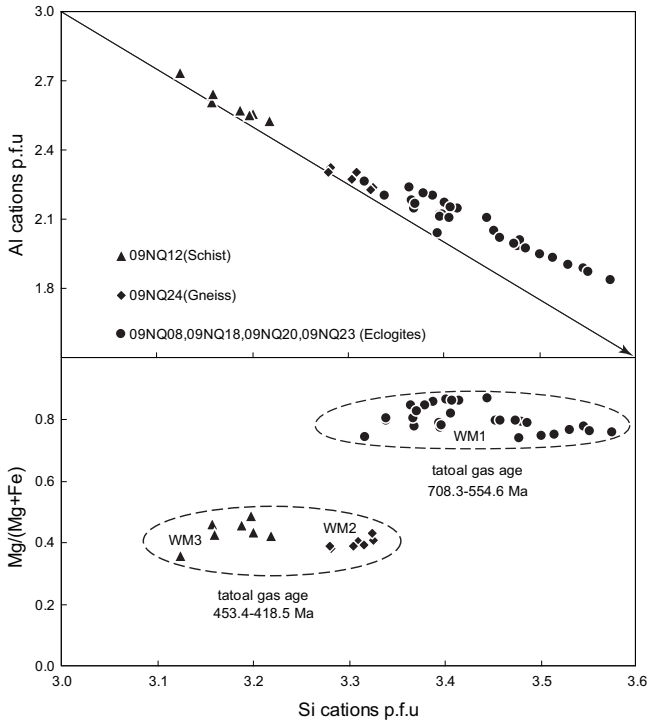

Figure 4.8 Si-Al-[Mg/(Fe+Mg)] diagram showing the main variations in Yuka white mica composition

Numerous scientists have documented that argon behavior in HP/UHP metamorphic mica is controlled by the mica mineral chemistry as well as by the lithology (Scaillet et al., 1992; Scaillet, 1996; Li et al., 1999; Di Vincenzo et al., 2001; Baxter et al., 2002; Di vincenzo et al., 2006). A combined ^{40}Ar/^{39}Ar bulk-sample stepwise heating and in situ spot mapping laser probe study on various phengites from the Dora-Maira nappe in the Western Alps leads the authors to argue that the Ar retentivity in phengite increases with its Mg content (Scaillet et al., 1992). This may suggest that the Ar retentivity in UHP metamorphic phengite from mafic and metapelitic rocks commonly shows a positive correlation with its Mg/Fe ratio. Accordingly, the influence of mica composition on Ar behaviour in phengite should be taken into account during the interpretation of phengite ^{40}Ar/^{39}Ar data from UHP metamorphic.

There are two possible sources of the extraneous ^{40}Ar in the Yuka eclogite phengite. First, it may originate from so-called "argon reservoirs" that are inferred to exist in the upper mantle or the crust and it may have been incorporated in phengite via fluid migration during the HP/UHP event (Arnaud and Kelley, 1995; Ruffet et al., 1995; Boundy et al., 1997; Wang et al., 2000b; El-Shazly et al., 2001).

Alternatively, the extraneous ^{40}Ar in eclogite phengite might be derived from the UHP eclogites and their protoliths. Eclogites from the Yuka area have basaltic protoliths with high Ti (TiO_2 2.4 – 3.4 wt. %) and K (K_2O 0.5 – 1.25 wt. %) combined with low Si (SiO_2 45 – 46 wt. %) and Mg (MgO 5 – 7 wt. %). They are rich in REE and LILE but depleted of HFSE. The geochemistry and REE patterns resemble those of within-plate basalt (WPB), enriched-type middle-ocean ridge basalt (E-MORB) and ocean island basalt (OIB) (Yang et al., 2006; Song et al., 2010), which generally have characteristics of low permeabilities and porosities (Smye et al., 2013). Primary amphibole is thought to be an important source for inherited ^{40}Ar in these ultramafic-mafic rocks that will not release its accumulated argon until under near- eclogite facies metamorphic conditions during subduction (Li et al., 1999; Li and Hou, 2001). Mafic protoliths may be maintained as "closed systems" with respect to advective solutions transported in the process of subduction and such lithologies may have been subject to inefficient removal and restricted transport of argon during the metamorphic cycle (Smye et al., 2013). Minerals such as WH1 phengite that formed under the peak UHP metamorphic conditions may retain their radiogenic argon partly or even almost completely, as it remained in such a relatively "closed" and "dry" UHP metamorphic geological environment during much of the metamorphic history of the rock (Scaillet et al., 1992; Scaillet, 1996; Giorgis et al., 2000; Sherlock and Kelley, 2002; Warren et al., 2012a; 2012c; Smye et al., 2013). It is interesting to note that neither individual apparent ages (475 – 797 Ma) nor total gas ages (555 – 708 Ma) of the mafic eclogite phengite separates are older than the 800 – 850 Ma ages of their protoliths (Zhang et al., 2005a; Yang et al., 2006; Chen et al., 2009a; Song et al., 2010). We conclude that the Yuka phengite extraneous ^{40}Ar is most reasonably explained as inherited ^{40}Ar.

4.5.2 Genesis of extraneous ^{40}Ar in Yuka amphibole

Amphibole samples from eclogites and garnet amphibolites from the Yuka terrane dated by $^{40}Ar/^{39}Ar$ stepwise heating also display pronounced discordant release spectra (Figure 4.2 and Figure 4.3). They have anomalously high initial apparent ages, unreasonably old total gas ages, gradually decreasing or crank-shaft shaped release patterns, as well as high initial $^{40}Ar/^{36}Ar$ ratios. All the evidence implies the existence of a heterogeneously distributed extraneous ^{40}Ar component. Like for UHP phengite from the same area, the extraneous ^{40}Ar in amphibole can also be derived from two origins: either inherited or excess ^{40}Ar.

As mentioned above, phengite in eclogite is mainly formed under "dry" UHP conditions, which is an essentially closed system with respect to argon. Amphibole, on the other hand, is formed under amphibolite-facies or even greenschist-facies retrograde stages and requires

the presence of aqueous fluid, which is normally derived from dehydration reactions of hydrous phases (Zheng, 2004; Hermann et al., 2006), crustal fluid flow or even meteoric water. During cooling, minerals such as biotite and K-feldspar with low Ar retentivities may continuously degas contributing to the K-derived ^{40}Ar concentration in the rock pile (Li et al., 1999; Li and Hou, 2001). This ^{40}Ar may dissolve into an aqueous fluid only if the temperature exceeds the closure temperature of these minerals for Ar. The resulting fluids with high ^{40}Ar partial pressures (P_{Ar}) could strongly influence the partitioning of argon into the retrograde amphibole. Specifically, Ar in aqueous fluid can be encapsulated by minerals during first growth and during later stages by crack-seal mechanisms, with the occurrences of secondary fluid inclusions (Kelley et al., 1986; Turner and Bannon, 1992; Harrison et al., 1993; Cumbest et al., 1994; Qiu and Wijbrans, 2006; 2008; Qiu et al., 2010).

Alternatively, if the rock hosting amphibole cools slowly and spends enough time at temperatures within its closure interval to Ar diffusion, a considerable amount of extraneous ^{40}Ar could diffuse into the mineral lattice via channelized fluid flow (Maboko et al., 1991; Di Vincenzo and Palmeri, 2001). Regardless the incorporation mechanism, extraneous ^{40}Ar with such an origin is excess rather than inherited ^{40}Ar.

4.5.3 Significance and interpretation of the new ^{40}Ar/^{39}Ar data

Due to the contamination of extraneous ^{40}Ar, part of the amphibole and phengite separates yields complex age spectra and often anomalous ages. Despite intensive efforts, several of the new ^{40}Ar/^{39}Ar results still not provide reasonably interpretable age results.

For some of the amphibole samples, the isotope correlation diagram (^{36}Ar/^{40}Ar vs. ^{39}Ar/^{40}Ar) can be applied to detect and quantitatively subtract extraneous ^{40}Ar from total ^{40}Ar (Figure 4.3). Isochron ages of amphibole imply that amphibolite-facies retrograde metamorphism occurred no later than ~472 Ma in the Yuka eclogites (see Figure 4.3). In other words, the UHP metamorphism of Yuka unit must have culminated before ~472 Ma, at least for some of the eclogites. The growth conditions of amphibole in garnet amphibolites (09NQ13 and 29) were estimated to be 540 ± 50 °C (for P = 7 ± 2 kbar, see Chapter 3), which corresponds to the commonly accepted closure temperature of amphibole (Harrison and McDougall, 1981; Villa, 1998). Thus, the isochron ages of ~ 472 Ma from the Yuka garnet amphibolites can be interpreted as cooling ages of a later amphibolite-facies metamorphic stage.

New ^{40}Ar/^{39}Ar analyses of muscovite/phengite in the host rocks from the Yuka terrane provide plateau ages of 418 Ma and 455 Ma (Figure 4.4, left) that are younger than reported zircon U-Pb ages of eclogite (485 – 495 Ma) (Zhang et al., 2005a) but consistent with previously reported ^{40}Ar/^{39}Ar ages of the host rocks (370 – 465 Ma) (Menold, 2006). It is interesting to note that the older plateau age of 455 Ma obtained from the well-preserved granitic gneiss (09NQ24Ph) has relatively high Si content (3.28 – 3.33 p.f.u), whereas a younger plateau age of 418 Ma comes from an intensively foliated schist (09NQ12Ms) with lower Si content (3.12 – 3.22 p.f.u). Recrystallization during greenschist facies metamorphism

and regional deformation cause these schist muscovites to release significant amounts of radiogenic ^{40}Ar resulting in younger plateau ages in these lower-Si muscovite crystals (Gouzu et al., 2006). Therefore, the plateau age of 418 Ma is taken as recording a greenschist-facies overprinting and associated penetrative ductile deformation. In contrast, the plateau age of 455 Ma recorded by the well-preserved gneiss muscovite probably dated post metamorphic cooling through muscovite closure temperature (450 ± 25 °C). The individual apparent ages from $^{40}Ar/^{39}Ar$ analyses of the Yuka eclogite phengites are apparently are not meaningful due to presence of extraneous ^{40}Ar, whereas the total gas age might be younger than, or close to their protolith ages (Qiu and Wijbrans, 2008).

K-feldspar from the Yuka granitic gneiss (09NQ24Kfs) is also contaminated by excess ^{40}Ar. Nonetheless, older apparent ages only show at low temperature steps, indicating that the excess ^{40}Ar was predominantly trapped in the adsorption sites or fluid inclusions (Harrison et al., 1994). The plateau age of ca. 283 Ma for the high temperature steps is interpreted as dating cooling through a temperature of 250 ± 25 °C.

4.5.4 Cooling history and exhumation mechanism

Petrologic, thermobarometric and geochronological studies in the Yuka terrane demonstrate that the relationship between eclogites and their host rocks is "*in situ*" rather than "tectonic emplacement" contacts (Zhang et al., 2003b). In other words, the rocks underwent early Paleozoic UHP metamorphism and subsequent exhumation together. Accordingly, although K-bearing minerals for $^{40}Ar/^{39}Ar$ dating in this study are extracted from either eclogites or their host rocks, respectively, they can still be used to construct pressure-temperature-time (*P-T-t*) and depth-time (*z-t*) paths using the closure temperatures for each of the radiogenic systems applied. Pressure to depth conversion will be calculated according to the assumed layered lithosphere model and lithostatic pressure (Hodges, 1991; Rubatto and Hermann, 2001): 20 km-thick upper crust, 10 km-thick lower crust followed by upper mantle with assumed densities of 2.7, 3.0 and 3.3 g/cm^3, respectively.

Since the maximum temperature that is experienced by the Yuka rocks (~730 °C) (Chen et al., 2005; Zhang et al., 2005a; Zhang et al., 2009b) is considerably lower than the closure temperature of Pb diffusion in zircon (>900 °C, Cherniak and Watson, 2001), and the zircon is formed during the UHP metamorphic event. Thus the published U-Pb zircon ages from Yuka eclogites are interpreted as the time of metamorphic crystallization/recrystallization. Combining existing zircon U-Pb data (Zhang et al., 2005a) with the new $^{40}Ar/^{39}Ar$ ages obtained in this study, simplified pressure-temperature-time (*P-T-t*) and depth-time (*z-t*) paths can be constructed by placing time marks at selected closure temperatures. As mentioned above, the growth conditions of amphiboles in garnet amphibolites (09NQ13 and 29) were estimated to be 540 ± 50 °C (for P = 7 ± 2 kbar, stage M4). In addition, the data points were plotted using an estimated argon diffusion closure temperature of 450 ± 25 °C for phengite (Kirschner et al., 1996; Villa, 1998; Harrison et al., 2009) and 300 ± 25 °C for K-feldspar (Heizler et al., 1988; McDougall and Harrison, 1999).

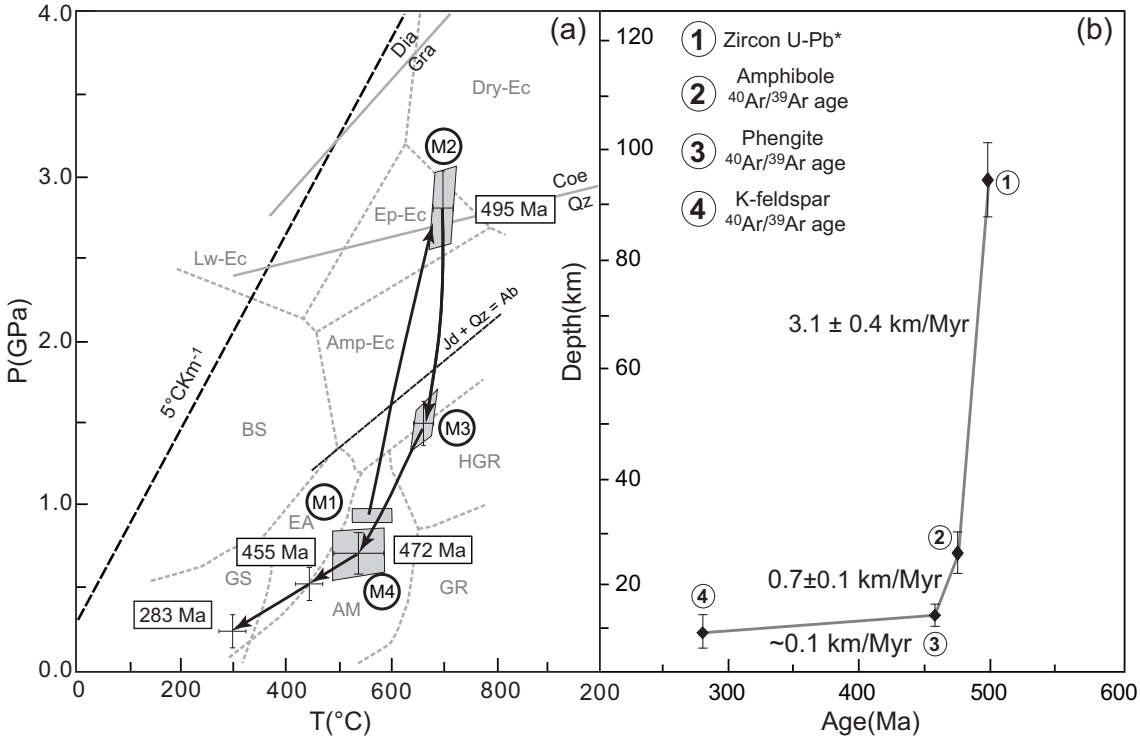

Figure 4.9 (a) Simplified *pressure-temperature-time (P-T-t)* path of the Yuka UHP terrane. M1: a pre-peak stage constrained by the inclusion assemblage in garnet cores in fresh eclogite. Conditions were obtained using a garnet-amphibole thermometer (Graham and Powell, 1984) and the Al_{total}-in amphibole barometer (Hollister et al., 1987). M2: a peak stage constrained by fresh eclogites. Conditions were obtained by garnet-clinopyroxene-phengite barometry (Waters and Martin, 1996) and garnet-phengite thermometry (Green and Hellman, 1982). M3: an initial retrograde stage constrained by retrogressed eclogite. Conditions were obtained using the garnet-biotite thermometer (Indares and Martignole, 1985) and in combination with the phengite barometer (Massonne and Szpurka, 1997). M4: a later retrograde stage constrained by garnet amphibolite for which *P-T* conditions were obtained using the garnet-amphibole thermometer (Graham and Powell, 1984) and the garnet-amphibole-plagioclase-(quartz) barometer (Kohn and Spear, 1990). (b) plot of depth *vs.* time (*z-t*) with exhumation volecities. The error bars on the age are too small to be shown. *Zircon U-Pb age of (1) from Zhang et al. (2005a), ^{40}Ar/^{39}Ar ages of (2) through (4) from this study.

As illustrated in Figure 4.9a, the UHP metamorphic rocks from the Yuka terrane experienced initial moderately fast cooling, followed by slow and very slow stages. In detail, the rocks cooled from the peak metamorphic conditions of about 730 °C to 540 ± 50 °C within 23 Ma, suggesting a cooling rate of ~7.4 °C/Myr. They cooled to ~450 °C within 17 Ma corresponding to cooling rate of ~5.3 °C/Myr and subsequent cooling from ~450 °C to ~300 °C proceeded at a rate of ~1 °C/Myr between 455 and 283 Ma.

The simplified depth-time path illustrates that the UHP rocks from the Yuka terrane were exhumed relatively rapidly from upper mantle depth to mid-crustal levels during an initial stage (Figure 4.9b). To be more precise, the Yuka UHP rocks have been exhumed at a

medium rate (3.1 ± 0.4 km/Myr) from an upper mantle depth of about 95 km beneath the earth surface at ~495 Ma to about 26 km in the lower-middle crust at ~472 Ma. Subsequently, the exhumation of Yuka terrane occurred in a much gentler at rates of 0.7 – 0.1 km/Myr to upper crust (~10 km).

The medium exhumation rate during the first stage may have been triggered by various dynamic mechanisms, such as reduced slab pull due to detachment between oceanic lithosphere and continental lithosphere ("slab-breakoff") (Davies and von Blanckenburg, 1995; Song et al., 2006), buoyancy-driven diapiric upwelling of the crustal materials through the mantle wedge (Yin et al., 2007) or flow along the subduction channel (Okay and Sengor, 1992; Engi et al., 2001). The subsequent period of gentle exhumation may have been primarily driven by underplating, erosion and assisted by oblique ductile extrusion under an extensional tectonic environment (Platt, 1993; Xu et al., 2006).

4.6 Conclusions

New phengite and amphibole $^{40}Ar/^{39}Ar$ dating results for the Yuka terrane in the North Qaidam UHP belt yield discordant release patterns, anomalously old apparent ages and non-atmospheric trapped Ar components. These signatures reflect contamination with extraneous ^{40}Ar: inherited or excess ^{40}Ar.

1. Extraneous ^{40}Ar in the UHP phengite demonstrates a close link between lithology and geochemical composition, and we suggest that is a locally derived component from their protolith (inherited ^{40}Ar). In contrast, extraneous ^{40}Ar in amphibole is probably primarily trapped in fluid inclusions and externally derived (excess ^{40}Ar).
2. Due to presence of excess ^{40}Ar, amphibole samples did not provide precise $^{40}Ar/^{39}Ar$ plateau ages to constrain the thermal evolution. However, isotope correlation diagrams suggest the amphibolite-facies overprinting of the Yuka eclogites took place around of ~472 Ma.
3. Combination of the new data with published zircon data (Zhang et al., 2005a) allows the construction of *P-T-t* and *z-t* paths that reveal that the Yuka UHP metamorphic rocks were exhumed from ~95 km to ~26 km with a moderate mean exhumation rate of 3.1 ± 0.4 km/Myr The subsequent exhumation to ~10 km with slow rates of ~0.7 − 0.1 km/Myr. The moderate initial exhumation scenarios may have been driven by slab breakoff, while the subsequent slow uplift was probably driven by erosion, underplating and lithospheric extension.